Nonlinear Poisson Effect Governed by a Mechanical Critical Transition

Jordan L. Shivers,[1,2] Sadjad Arzash,[1,2] and F. C. MacKintosh[1,2,3,*]
[1]Department of Chemical and Biomolecular Engineering, Rice University, Houston, Texas 77005, USA
[2]Center for Theoretical Biological Physics, Rice University, Houston, Texas 77030, USA
[3]Departments of Chemistry and Physics and Astronomy, Rice University, Houston, Texas 77005, USA

(Received 5 August 2019; published 23 January 2020)

Under extensional strain, fiber networks can exhibit an anomalously large and nonlinear Poisson effect accompanied by a dramatic transverse contraction and volume reduction for applied strains as small as a few percent. We demonstrate that this phenomenon is controlled by a collective mechanical phase transition that occurs at a critical uniaxial strain that depends on network connectivity. This transition is punctuated by an anomalous peak in the apparent Poisson's ratio and other critical signatures such as diverging nonaffine strain fluctuations.

DOI: 10.1103/PhysRevLett.124.038002

When an elastic body is subjected to an infinitesimal strain $\varepsilon_{\parallel}$ along one axis, the corresponding strain $\varepsilon_{\perp}$ in the transverse direction(s) defines Poisson's ratio $\nu = -\varepsilon_{\perp}/\varepsilon_{\parallel}$ [1,2]. Although this ratio is constrained to the range $\nu \in [-1, 1/2]$ for isotropic materials in three dimensions (3D), there have been numerous recent reports of anomalously large apparent Poisson's ratios exceeding $1/2$ in a variety of fibrous materials at small strain, including felt [3] and networks of collagen [4–8] and fibrin [7,9]. This corresponds to an anomalous reduction in volume under extension, in apparent stark contrast to the linear behavior of all isotropic materials, which strictly maintain or increase their volume under infinitesimal extension. This is even true of auxetic materials with $\nu < 0$ [10–13]. A volume reduction under uniaxial extension can have dramatic effects in living tissue, such as the development of highly aligned, stiffened network regions with reduced porosity between contractile cells in the extracellular matrix [4,8,14,15]. Although it has been argued that this effect is related to stiffening and other nonlinear phenomena in such networks [3,8,16], it remains unclear to what extent this anomaly is controlled by network architecture and filament properties.

Here, we show that the anomalous Poisson's ratio of fiber networks is governed by a mechanical phase transition induced by applied axial strain. Using simulations of disordered networks in two dimensions (2D) and 3D, we show that this phenomenon is critical in nature, with diverging strain fluctuations in the vicinity of the transition and a corresponding maximum of the apparent Poisson's ratio. Connecting with recent studies of mechanical criticality in athermal networks [17–22], we demonstrate that this maximum occurs at a connectivity-controlled strain corresponding to a macroscopic crossover between distinct mechanical regimes, with large-scale, collective network rearrangements as a branched, system-spanning network of tensile force chains develops. Our results highlight the influence of collective properties on the nonlinear mechanics of athermal networks and suggest that controlling connectivity could enable the design of tailored elastic anomalies in engineered fiber networks.

Recent work has demonstrated that the strain-stiffening effect in cross-linked networks of stiff athermal semiflexible biopolymers, such as collagen, which can be modeled as elastic rods with bending modulus κ and stretching modulus μ, can be understood as a mechanical phase transition between a bending-dominated regime and a stretching-dominated regime at an applied shear or extensional strain governed by the average network connectivity z [18–20,23]. Despite being athermal, such networks exhibit classic signatures of criticality near this transition, including power-law scaling of the elastic moduli with strain and system-size-dependent nonaffine strain fluctuations indicative of a diverging correlation length [18,20]. In the limit of $\kappa \to 0$, stiffening corresponds to the rearrangement of the network to form a marginally stable, highly heterogenous network of branched force chains [24,25] similar to the force networks observed in marginal jammed packings under compressive or shear strain [26–28]. Prior work has considered this rigidity transition in networks under applied simple shear [18,20–22] or bulk strain [21–23], with quantitative agreement between shear experiments on collagen and simulations [29].

We find that an analogous collective mechanical phase transition controls the mechanics of networks under uniaxial strain with free orthogonal strains. In athermal semiflexible polymer networks, strain stiffening and the nonlinear Poisson effect occur at a critical extensional strain controlled by network connectivity, corresponding to a transition from a bending-dominated regime to one dominated by stretching. The expected phase diagram in connectivity-strain space is sketched in Fig. 1(a). As applied strain drives a network to

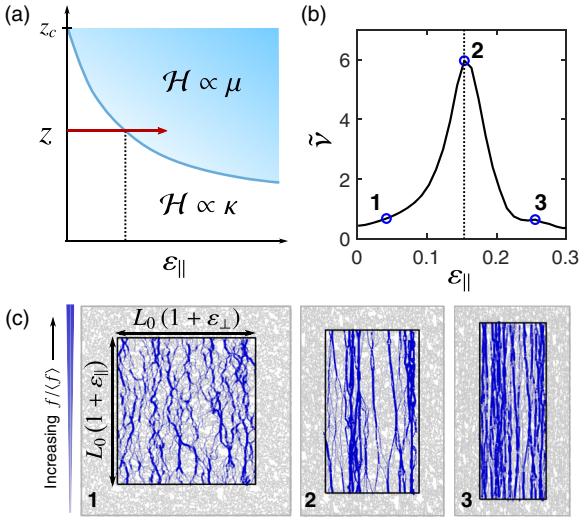

FIG. 1. (a) Under applied extensional strain $\varepsilon_\parallel$ (red arrow) with free transverse strains, subisostatic ($z < z_c$) athermal fiber networks transition from a soft, bending-dominated regime ($\mathcal{H} \propto \kappa$, floppy in the limit of $\kappa \to 0$) to a stiff, stretching-dominated regime ($\mathcal{H} \propto \mu$) at a critical applied strain $\varepsilon_{\parallel,c}$ (dotted line) that increases with decreasing z. As $z \to z_c$, $\varepsilon_{\parallel,c} \to 0$. (b) The incremental Poisson's ratio $\tilde{\nu} = -\partial\varepsilon_\perp/\partial\varepsilon_\parallel$ exhibits a peak at the critical strain, indicated by the dotted line. The black curve corresponds to a 2D packing-derived (PD) network with $\tilde{\kappa} = 10^{-5}$ and $z = 3.2$. Network configurations corresponding to the numbered circles are shown in (c). Here, the black box represents the deformation of the initially square periodic boundaries. Bonds under greater tension f than the average, $\langle f \rangle$, are colored blue with thickness proportional to $f/\langle f \rangle$.

approach and cross the critical strain boundary, the network's mechanics become stretching dominated and the resultant nonlinear strain stiffening induces dramatic transverse contraction coinciding with a peak in the incremental Poisson's ratio $\tilde{\nu}$ [see Fig. 1(b)]. Concurrent with this transition, the system exhibits nonaffine strain fluctuations that grow by orders of magnitude as criticality is approached (either by decreasing κ or approaching the critical strain). We demonstrate that this phenomenon occurs irrespective of the details of the underlying network structure, consistent with past observations of networks under simple shear [18,25]. Our results suggest that the dramatic nonlinear Poisson effect observed in collagen and fibrin gels is macroscopic evidence of this critical rigidity transition.

Models.—We consider 2D and 3D disordered networks comprising interconnected one-dimensional Hookean springs with stretching modulus μ, with additional bending interactions with modulus κ between adjacent bonds. To explore the influence of network structure on the transition, we test a variety of network geometries, including Mikado networks [30], 2D and 3D jammed PD networks [25], 3D Voronoi networks [16], and 3D random geometric graph networks [31,32]. The network Hamiltonian $\mathcal{H} = \mathcal{H}_s + \mathcal{H}_b$ consists of a stretching contribution,

$$\mathcal{H}_s = \frac{\mu}{2}\sum_{ij}\frac{(\ell_{ij} - \ell_{ij,0})^2}{\ell_{ij,0}}, \tag{1}$$

in which the sum is taken over connected node pairs ij, ℓ_{ij} is the length of the bond connecting nodes i and j, and $\ell_{ij,0}$ is the corresponding rest length, as well as a bending contribution,

$$\mathcal{H}_b = \frac{\kappa}{2}\sum_{ijk}\frac{(\theta_{ijk} - \theta_{ijk,0})^2}{\ell_{ijk,0}}, \tag{2}$$

in which the sum is taken over connected node triplets ijk, θ_{ijk} is the angle between bonds ij and jk, $\theta_{ijk,0}$ is the corresponding rest angle, and $\ell_{ijk,0} = (\ell_{ij,0} + \ell_{jk,0})/2$. For Mikado networks, which we designate to have freely hinging cross links, the sum in Eq. (2) is taken only over consecutive node triplets along initially collinear bonds. Following prior work, we set $\mu = 1$ and vary the dimensionless bending rigidity $\tilde{\kappa} = \kappa/(\mu\ell_c^2)$ [25,39], where ℓ_c is the average bond length. Since the volume fractions of biopolymer gels are typically 1% or less [29,40], we do not include excluded volume effects in the results presented below, although we examine their effects in Supplemental Material [32]. All network models utilize generalized Lees-Edwards periodic boundary conditions [25,41], which specify that the displacement vectors between each network node and its periodic images transform according to the deformation gradient tensor Λ. We consider purely extensional strain, with $\Lambda_{ii} = 1 + \varepsilon_i$, where ε_i is the strain along the i axis relative to the initial configuration. Whereas the primary results of this Letter utilize periodic boundaries, we have also performed simulations of nonperiodic networks with fixed upper and lower boundaries. We find that fixed boundaries of width equal to or greater than the sample length can suppress the apparent Poisson's ratio [32]. The normal stress components σ_{ii} are computed as $\sigma_{ii} = (\partial\mathcal{H}/\partial\varepsilon_i)/V$, in which V is the system's volume. Unless otherwise stated, all curves correspond to an average over 15 samples.

To measure the nonlinear Poisson effect, we apply quasistatic longitudinal extensional strain $\varepsilon_\parallel \equiv \varepsilon_1$ in small increments $\delta\varepsilon_\parallel = \varepsilon_{\parallel,n} - \varepsilon_{\parallel,n-1}$ and, at a given strain, first allow the system to reach mechanical equilibrium by minimizing the network's Hamiltonian using the L-BFGS algorithm [42]. After each extensional strain step, we simulate free transverse boundaries by incrementally varying the transverse strain(s) ε_2 (and ε_3 in 3D) in order to reduce the corresponding transverse normal stress component(s) to 0, i.e., $|\partial\mathcal{H}/\partial\varepsilon_i| \approx 0$. In 2D the single transverse strain is $\varepsilon_\perp \equiv \varepsilon_2$, whereas in 3D the stresses along the two transverse axes are relaxed independently and we define the transverse strain, for the purposes of computing the incremental Poisson's ratio, as $\varepsilon_\perp \equiv (\varepsilon_2 + \varepsilon_3)/2$. For orientationally isotropic network models, ε_2 and ε_3 are

equivalent in the limit of large system size. The differential Young's modulus $\tilde{E}$ is computed as $\tilde{E} = \partial\sigma_{\parallel}/\partial\varepsilon_{\parallel}$.

Results.—Subisostatic athermal networks undergo a transition from a bending-dominated regime to a stiff stretching-dominated regime at a critical applied shear or extensional strain [43,44]. Recent work showed that athermal networks under extensional strain with free transverse strains, which we consider in this work, undergo a similar transition from a bending-dominated to stretching-dominated regime corresponding with strain stiffening [16]. To examine the influence of bending rigidity on this transition, we first consider 2D packing-derived networks with fixed connectivity $z = 3.2 < z_c$ and varying reduced bending rigidity $\tilde{\kappa}$. In Fig. 2(a), we plot the relaxed transverse strain $\varepsilon_{\perp}$ as a function of applied longitudinal extensional strain $\varepsilon_{\parallel}$, with the corresponding incremental Poisson's ratio $\tilde{\nu} = -\partial\varepsilon_{\perp}/\partial\varepsilon_{\parallel}$ shown in Fig. 2(b). The

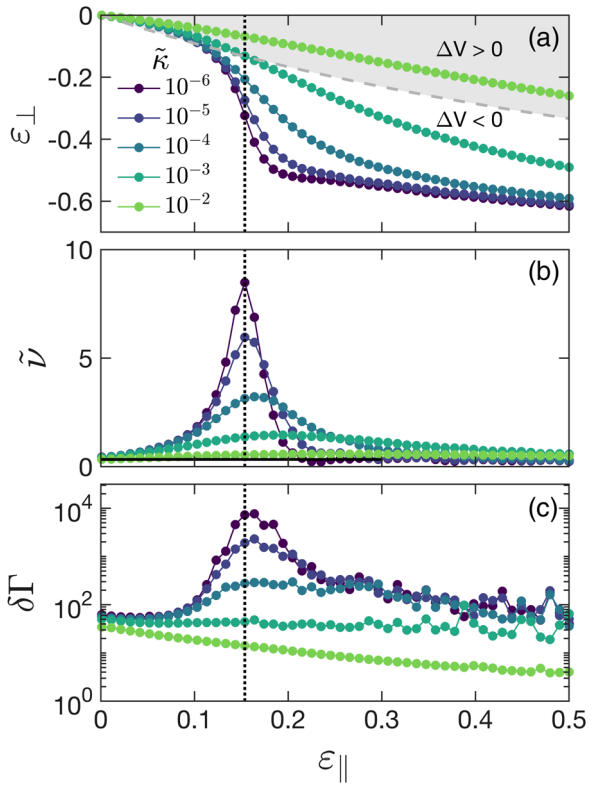

FIG. 2. (a) Relaxed transverse strain $\varepsilon_{\perp}$ as a function of applied extensional strain $\varepsilon_{\parallel}$ for 2D packing-derived networks with $z = 3.2$ and varying $\tilde{\kappa}$. For large $\tilde{\kappa}$, networks deform linearly up to relatively large strains. The gray dashed line corresponds to constant volume, $\Delta V \equiv V - V_0 = 0$. In the limit of low $\tilde{\kappa}$, networks deform linearly at low strains, with a linear Poisson's ratio less than 1, but exhibit a significant increase in transverse contraction at a critical strain $\varepsilon_{\parallel,c}$, indicated by the dotted black line. (b) The magnitude of the incremental Poisson's ratio $\tilde{\nu} = -\partial\varepsilon_{\perp}/\partial\varepsilon_{\parallel}$ peaks at the critical strain and increases with decreasing $\tilde{\kappa}$. (c) At the critical strain, we observe a corresponding peak in the nonaffine strain fluctuations $\delta\Gamma$ that increases in magnitude as $\tilde{\kappa}$ is decreased.

fraction of the total network energy due to bending interactions $\mathcal{H}_b/\mathcal{H}$ as a function of strain is shown in Supplemental Material [32]. Networks with high $\tilde{\kappa}$ deform approximately linearly up to relatively large applied strains, with minimal strain dependence of $\tilde{\nu}$. In contrast, networks with low $\tilde{\kappa}$ exhibit similar linear deformation (with $\tilde{\nu} < 1$) in the limit of small applied strain, but under increasing applied strain these undergo a transition to a much stiffer stretching-dominated regime, resulting in significant transverse contraction and thus a very large apparent Poisson's ratio. At larger strains, within the stretching-dominated regime, the networks again deform approximately linearly with an incremental Poisson's ratio $\tilde{\nu} < 1$. The transition occurs at a critical applied extension ε_c, which we define as the strain corresponding to the inflection point in the $\varepsilon_{\perp}$ vs $\varepsilon_{\parallel}$ curve as $\kappa \to 0$. By definition, this corresponds to a peak in $\tilde{\nu}$, which grows with decreasing $\tilde{\kappa}$.

This unusual nonlinear Poisson effect results from the asymmetric nonlinear mechanics of these networks, which stiffen dramatically under extensional strain but remain soft under compression [3,4]. Compressing a semiflexible polymer network induces normal stresses proportional to the bending rigidity κ of the constituent polymers, whereas sufficient extension induces normal stresses proportional to the polymer stretching modulus μ [43]. An athermal network under uniaxial extension with *fixed* transverse strains exhibits an increase in the magnitude of its normal stresses from $\sigma_{ii} \propto \kappa$ to $\sigma_{ii} \propto \mu$ at the critical strain, both along the strain axis ($\sigma_{\parallel}$) and the transverse axes ($\sigma_{\perp}$). Relaxing the transverse boundaries to satisfy $\sigma_{\perp} = 0$ requires contraction along the transverse axes, which necessarily reduces the stiff stretching-induced contributions ($\propto \mu$) until these are balanced by softer, compression-induced contributions ($\propto \kappa$). The amount of transverse contraction in the vicinity of the critical strain thus increases with μ/κ.

Past work showed that athermal networks under applied shear strain exhibit diverging nonaffine strain fluctuations at the critical strain, in the limit of $\tilde{\kappa} \to 0$, indicative of a diverging correlation length [18,20,45]. Concurrent with the strain-driven transition in this work, we observe similarly large internal strain fluctuations. We use an analogous measure of the strain fluctuations for the deformation gradient tensor $\mathbf{\Lambda}$ defined above. For the nth strain step, the incremental applied extensional strain $\delta\varepsilon_{\parallel} = \varepsilon_{\parallel,n} - \varepsilon_{\parallel,n-1}$ and relaxation of the transverse strain(s) transforms the deformation gradient tensor from $\mathbf{\Lambda}_{n-1}$ to $\mathbf{\Lambda}_n$. We compute the resulting differential nonaffinity $\delta\Gamma$ as

$$\delta\Gamma = \frac{1}{\ell_c^2(\delta\varepsilon_{\parallel})^2}\langle\|\delta\mathbf{u}_i - \delta\mathbf{u}_i^{\text{aff}}\|^2\rangle \tag{3}$$

in which the average is taken over all nodes i, ℓ_c is the initial average bond length, $\delta\mathbf{u}_i = \mathbf{u}_{i,n} - \mathbf{u}_{i,n-1}$ is the actual displacement of node i after the extensional strain step and

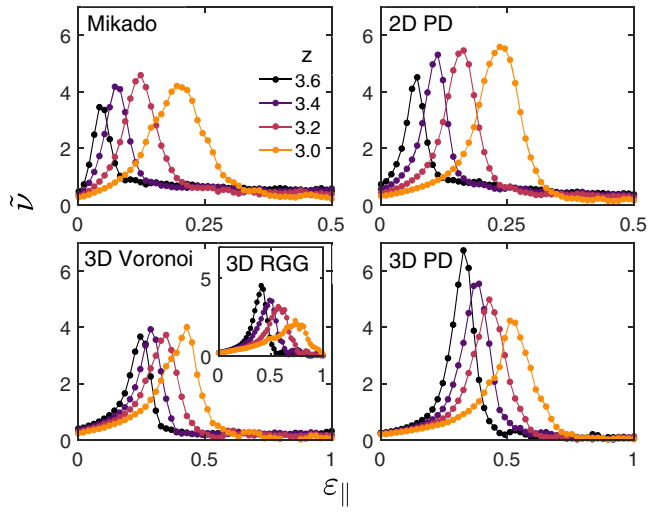

FIG. 3. Incremental Poisson's ratio $\tilde{\nu} = -\partial\varepsilon_{\perp}/\partial\varepsilon_{\|}$ as a function of applied extensional strain $\varepsilon_{\|}$ for various 2D and 3D network structures, as labeled in the top right of each panel, with varying connectivity z. In all networks, the critical strain $\varepsilon_{\|,c}$, corresponding to the peak in $\tilde{\nu}$, increases with decreasing z.

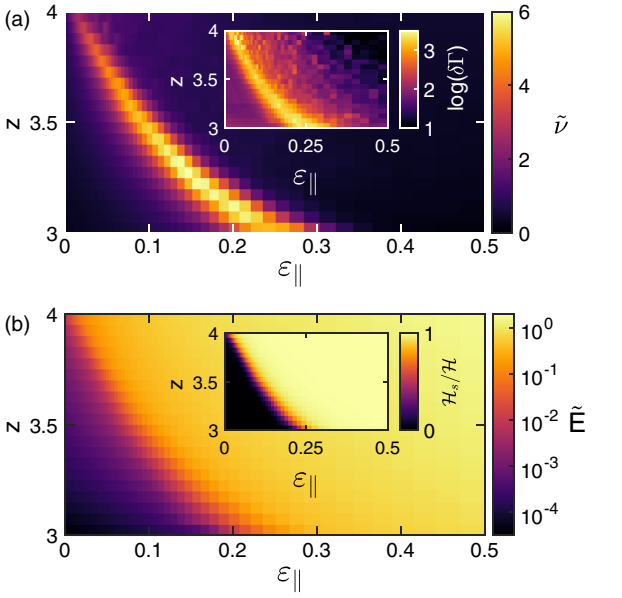

FIG. 4. (a) Incremental Poisson's ratio $\tilde{\nu} = -\partial\varepsilon_{\perp}/\partial\varepsilon_{\|}$ as a function of applied extensional strain $\varepsilon_{\|}$ and average connectivity z for 2D packing-derived networks with $W = 100$ and $\tilde{\kappa} = 10^{-5}$. Inset: For a given connectivity z, the differential nonaffinity $\delta\Gamma$ exhibits a peak coinciding with the peak in the incremental Poisson ratio $\tilde{\nu}$. (b) Differential Young's modulus $\tilde{E} = \partial\sigma_{\|}/\partial\varepsilon_{\|}$ for the same networks as in (a). Inset: Corresponding stretching energy fraction $\mathcal{H}_s/\mathcal{H}$.

transverse strain relaxation, and $\delta\mathbf{u}_i^{\text{aff}}$ is the displacement of node i corresponding to an affine transformation from the previous configuration at strain state Λ_{n-1} to the new strain state $\mathbf{\Lambda}_n$. Consistent with prior work examining networks under shear strain [20], we find that increasing $\tilde{\kappa}$ results in increasingly affine deformation (decreasing $\delta\Gamma$), whereas in the low-$\tilde{\kappa}$ limit we observe a peak in $\delta\Gamma$ at the critical strain that grows with decreasing $\tilde{\kappa}$ [see Fig. 2(c)].

For athermal subisostatic networks under applied simple shear strain, the critical strain is governed by the average network connectivity z [18,45,46], with the critical strain decreasing to 0 as z approaches the Maxwell isostatic value $z_c = 2d$, where d is the dimensionality [47]. As sketched in our hypothesized phase diagram [see Fig. 1(a)], we expect z to similarly control the critical strain for networks under extensional strain with free orthogonal strains. In Fig. 3, we plot the incremental Poisson ratio $\tilde{\nu}$ as a function of $\varepsilon_{\|}$ for several network geometries in 2D and 3D with varying z. While the precise location of the critical strain for a given connectivity is sensitive to the choice of network structure, we find that all networks tested exhibit behavior that is qualitatively consistent with the proposed phase diagram, with a critical strain $\varepsilon_{\|,c}$ that decreases as $z \to z_c$.

We also explicitly map out a phase diagram for packing-derived networks in 2D. In Fig. 4(a), we plot both the incremental Poisson's ratio $\tilde{\nu}$ and differential nonaffinity $\delta\Gamma$ for 2D PD networks as a function of applied strain over a range of z values up to the 2D isostatic point, $z_c = 4$. Both quantities become maximal at a critical strain that approaches 0 as $z \to z_c$. Near z_c, the critical strain grows as $\varepsilon_{\|,c} \propto z_c - z$, consistent with prior results [23,32,46]. We plot the corresponding differential Young's modulus $\tilde{E} = \partial\sigma_{\|}/\partial\varepsilon_{\|}$ as a function of z and $\varepsilon_{\|}$ in Fig. 4(b), demonstrating that the transition of the network from the soft, bending-dominated regime ($\tilde{E} \propto \kappa$) to the stiffer, stretching-dominated regime ($\tilde{E} \propto \mu$) coincides with peaks in both the incremental Poisson's ratio and the differential nonaffinity [Fig. 4(a)]. Further, we find that the differential Young's modulus scales as a power law $\tilde{E} \propto |\varepsilon_{\|} - \varepsilon_{\|,c}|^f$ above the critical strain [32].

Discussion.—We have demonstrated that the nonlinear Poisson effect observed in subisostatic networks is a direct consequence of a strain-driven collective mechanical phase transition. Whereas the large apparent Poisson's ratios observed in such networks at finite strains can be qualitatively understood as resulting from their highly asymmetric mechanical properties, i.e., that they stiffen dramatically under finite extension but remain comparatively soft under compression, as discussed conceptually in Refs. [3,4], we have demonstrated that this asymmetry becomes maximized at a critical phase boundary controlled by strain and connectivity. At this boundary, a network exhibits diverging strain fluctuations as it collectively rearranges to transition from a soft, bending-dominated regime to a stiff, stretching-dominated regime. In the latter, marginally stable state, the mechanics become dominated by an underlying branched network of bonds under tension, which generates tensile transverse normal stresses that drive the lateral contraction of the network against the weaker compression-induced stresses. This results in an

apparent Poisson's ratio that exceeds $1/2$ at the phase transition and grows as a function of the relative magnitude the stiff and soft contributions, μ/κ. Whereas we have focused on the $T = 0$ limit with an eye towards networks such as collagen, we note that finite temperature can stabilize otherwise floppy networks [48,49] and would be expected to reduce the peak in the differential Poisson's ratio in a manner similar to finite κ.

Using simulations of a variety of network architectures in 2D and 3D, we have shown that this effect is robustly controlled by connectivity and occurs independently of the precise underlying network structure. Further, we have demonstrated critical scaling of the differential Young's modulus [32] similar to what has been shown for the shear modulus of collagen networks [18]. This suggests that experimental measurements of the differential Young's modulus of collagen gels under uniaxial strain should quantitatively fit the predicted scaling form, with a given sample exhibiting a peak in the incremental Poisson's ratio at the transition point. Further work could enable prediction of the local stiffness in the extracellular matrix based on the observed local strain asymmetry.

This work was supported in part by the National Science Foundation Division of Materials Research (Grant No. DMR-1826623) and the National Science Foundation Center for Theoretical Biological Physics (Grant No. PHY-1427654). J. L. S. acknowledges additional support from the Ken Kennedy Institute Graduate Fellowship and the Riki Kobayashi Fellowship in Chemical Engineering.

*Corresponding author.
fcmack@gmail.com

[1] S. D. Poisson, Annls Chim. Phys. **36**, 384 (1827).
[2] L. D. Landau and E. M. Lifshitz, in *Theory of Elasticity*, Course of Theoretical Physics (Pergamon Press, Oxford, 1959).
[3] A. Kabla and L. Mahadevan, J. R. Soc. Interface **4**, 99 (2007).
[4] D. Vader, A. Kabla, D. Weitz, and L. Mahadevan, PLoS One **4**, e5902 (2009).
[5] B. A. Roeder, K. Kokini, and S. L. Voytik-Harbin, J. Biomech. Eng. **131**, 31004 (2009).
[6] S. P. Lake and V. H. Barocas, Ann. Biomed. Eng. **39**, 1891 (2011).
[7] J. Steinwachs, C. Metzner, K. Skodzek, N. Lang, I. Thievessen, C. Mark, S. Münster, K. E. Aifantis, and B. Fabry, Nat. Methods **13**, 171 (2016).
[8] E. Ban, H. Wang, J. M. Franklin, J. T. Liphardt, P. A. Janmey, and V. B. Shenoy, Proc. Natl. Acad. Sci. U.S.A. **116**, 6790 (2019).
[9] A. E. X. Brown, R. I. Litvinov, D. E. Discher, P. K. Purohit, and J. W. Weisel, Science **325**, 741 (2009).
[10] G. N. Greaves, A. L. Greer, R. S. Lakes, and T. Rouxel, Nat. Mater. **10**, 823 (2011).
[11] L. A. Mihai and A. Goriely, Proc. R. Soc. A **470**, 20140363 (2014).
[12] D. R. Reid, N. Pashine, J. M. Wozniak, H. M. Jaeger, A. J. Liu, S. R. Nagel, and J. J. de Pablo, Proc. Natl. Acad. Sci. U.S.A. **115**, E1384 (2018).
[13] R. Rens and E. Lerner, arXiv:1904.07054.
[14] H. Wang, A. S. Abhilash, C. S. Chen, R. G. Wells, and V. B. Shenoy, Biophys. J. **107**, 2592 (2014).
[15] A. S. Abhilash, B. M. Baker, B. Trappmann, C. S. Chen, and V. B. Shenoy, Biophys. J. **107**, 1829 (2014).
[16] R. C. Picu, S. Deogekar, and M. R. Islam, J. Biomech. Eng. **140**, 021002 (2018).
[17] C. P. Broedersz, X. Mao, T. C. Lubensky, and F. C. MacKintosh, Nat. Phys. **7**, 983 (2011).
[18] A. Sharma, A. J. Licup, K. A. Jansen, R. Rens, M. Sheinman, G. H. Koenderink, and F. C. MacKintosh, Nat. Phys. **12**, 584 (2016).
[19] J. Feng, H. Levine, X. Mao, and L. M. Sander, Soft Matter **12**, 1419 (2016).
[20] J. L. Shivers, S. Arzash, A. Sharma, and F. C. MacKintosh, Phys. Rev. Lett. **122**, 188003 (2019).
[21] R. Rens, C. Villarroel, G. Düring, and E. Lerner, Phys. Rev. E **98**, 062411 (2018).
[22] M. Merkel, K. Baumgarten, B. P. Tighe, and M. L. Manning, Proc. Natl. Acad. Sci. U.S.A. **116**, 6560 (2019).
[23] M. Sheinman, C. P. Broedersz, and F. C. MacKintosh, Phys. Rev. E **85**, 021801 (2012).
[24] C. Heussinger and E. Frey, Eur. Phys. J. E **24**, 47 (2007).
[25] J. L. Shivers, J. Feng, A. Sharma, and F. C. MacKintosh, Soft Matter **15**, 1666 (2019).
[26] F. Radjai, M. Jean, J. J. Moreau, and S. Roux, Phys. Rev. Lett. **77**, 274 (1996).
[27] C. S. O'Hern, S. A. Langer, A. J. Liu, and S. R. Nagel, Phys. Rev. Lett. **86**, 111 (2001).
[28] T. S. Majmudar and R. P. Behringer, Nature (London) **435**, 1079 (2005).
[29] K. A. Jansen, A. J. Licup, A. Sharma, R. Rens, F. C. MacKintosh, and G. H. Koenderink, Biophys. J. **114**, 2665 (2018).
[30] D. A. Head, A. J. Levine, and F. C. MacKintosh, Phys. Rev. Lett. **91**, 108102 (2003).
[31] F. Beroz, L. M. Jawerth, S. Münster, D. A. Weitz, C. P. Broedersz, and N. S. Wingreen, Nat. Commun. **8**, 16096 (2017).
[32] See Supplemental Material at http://link.aps.org/supplemental/10.1103/PhysRevLett.124.038002, which includes Refs. [33–38], for details on network generation and sample configurations, discussion of buckling, boundary conditions, and excluded volume effects, and additional evidence of the bending-to-stretching transition, critical exponents, and shape of the phase boundary for packing-derived networks.
[33] J. Wilhelm and E. Frey, Phys. Rev. Lett. **91**, 108103 (2003).
[34] C. O'Hern, L. Silbert, and S. Nagel, Phys. Rev. E **68**, 011306 (2003).
[35] M. van Hecke, J. Phys. Condens. Matter **22**, 033101 (2010).
[36] S. Dagois-Bohy, B. P. Tighe, J. Simon, S. Henkes, and M. van Hecke, Phys. Rev. Lett. **109**, 095703 (2012).
[37] D. J. Koeze, D. Vågberg, B. B. Tjoa, and B. P. Tighe, Europhys. Lett. **113**, 54001 (2016).

[38] The CGAL Project, *CGAL User and Reference Manual*, 5th ed. (CGAL Editorial Board, 2019), https://doc.cgal.org/5.0/Manual/packages.html.
[39] A. J. Licup, S. Münster, A. Sharma, M. Sheinman, L. M. Jawerth, B. Fabry, D. A. Weitz, and F. C. MacKintosh, Proc. Natl. Acad. Sci. U.S.A. **112**, 9573 (2015).
[40] S. Motte and L. J. Kaufman, Biopolymers **99**, 35 (2013).
[41] A. W. Lees and S. F. Edwards, J. Phys. C **5**, 1921 (1972).
[42] J. Nocedal and S. J. Wright, *Numerical Optimization*, 2nd ed. (Springer Science & Business Media, New York, NY, USA, 2006).
[43] M. Vahabi, A. Sharma, A. J. Licup, A. S. G. van Oosten, P. A. Galie, P. A. Janmey, and F. C. MacKintosh, Soft Matter **12**, 5050 (2016).
[44] A. J. Licup, A. Sharma, and F. C. MacKintosh, Phys. Rev. E **93**, 012407 (2016).
[45] A. Sharma, A. J. Licup, R. Rens, M. Vahabi, K. A. Jansen, G. H. Koenderink, and F. C. MacKintosh, Phys. Rev. E **94**, 042407 (2016).
[46] M. Wyart, H. Liang, A. Kabla, and L. Mahadevan, Phys. Rev. Lett. **101**, 215501 (2008).
[47] J. C. Maxwell, London Edinburgh Dublin Philos. Mag. J. Sci. **27**, 294 (1864).
[48] M. Dennison, M. Sheinman, C. Storm, and F. C. MacKintosh, Phys. Rev. Lett. **111**, 095503 (2013).
[49] L. Zhang and X. Mao, Phys. Rev. E **93**, 022110 (2016).